J. Fluid Mech. (1978), *vol.* 88, *part* 3, *pp.* 485–497
Printed in Great Britain

Hydrodynamic propulsion by large amplitude oscillation of an airfoil with chordwise flexibility

By J. KATZ AND D. WEIHS

Department of Aeronautical Engineering, Technion–Israel Institute of Technology, Haifa

(Received 8 February 1978)

The hydrodynamic forces due to the motion of a flexible foil in a large amplitude curved path in an inviscid incompressible flow are analysed. A parametric study of large amplitude oscillatory propulsion, with special emphasis on the effect of chordwise flexibility of the fin, is presented. This flexibility was found to increase the propulsive efficiency by up to 20 % while causing small decreases in the overall thrust, compared with similar motion with rigid foils.

1. Introduction

Aquatic propulsion by means of oscillating thin foils has been the focus of considerable interest in the last two decades. This is due to the relatively high efficiency obtainable by such systems and other advantages like scaling possibilities (limited in propellers owing to the tip-speed problem) and low-noise characteristics.

The high efficiency obtainable by such propulsion systems has been pointed out in various studies, including Lighthill (1960), Wu (1961), Bonthron & Fejer (1962) and Siekmann (1962, 1963). Experimental proof was presented by Webb (1975), who estimated the propulsive efficiency of fish swimming by this technique to be around 80 %. Scherer (1968) built an undulating propulsor which included a rigid plate of aspect ratio 3. His results show that the efficiency and thrust coefficient of his propulsor are competitive with those of classical rotating propellers.

The first mathematical models analysing the oscillatory propulsion of fishes were based on small amplitude potential theory (e.g. Lighthill 1960; Wu 1961). However, it is clear from the work of Scherer (1968) and Chopra (1976) as well as from observations of aquatic creatures that in order to achieve practical thrust levels the oscillation amplitude of the propulsor foil must be large compared with its chord.

Various possible mathematical methods for dealing with large amplitude motion of high aspect ratio foils have been put forward. Thus the arbitrary potential motion of a thick two-dimensional airfoil was treated by the doublet lattice method in Giesing's (1968) work. James (1973) analysed circular and harmonic motions of an airfoil by means of the acceleration potential, while Chopra (1976) solved the large amplitude harmonic oscillation case with the aid of the impulse approach. All of the studies mentioned dealt with rigid foils. In many cases where oscillatory propulsion is used, however (e.g. fish lunate tails, swim fins), the fin chord is flexible and the oscillatory motion has an amplitude of the order of magnitude of the fin chord. Therefore the present study develops a general method, within the limitations of two-dimensional theory,

for solving the motion of flexible surfaces moving in curved paths (limited to angles of attack such that no flow separation occurs and to non-self-intersecting trajectories).

In the present work only passive flexibility is included. The method proposed can include foil shape changes by design, and this is in fact the basis of a further study being carried out currently where optimal foil curvatures as a function of time and trajectory are to be obtained.

2. General theory of the motion of a flexible surface

Consider a thin foil with a flexible chord of constant length c which varies its shape passively owing to the hydrodynamical forces acting on it. The propulsor is taken to move in water at high Reynolds number so that the analysis can be based on incompressible potential theory (Lighthill 1971; James 1973; Chopra 1976). A given point P on the foil (at the leading edge in the present study) is forced to follow a predetermined path $S(S_{x^*}, S_{z^*})$ (figure 1). The trajectory S is such that the flow disturbance caused by the foil stays small and no point of the foil traverses the wake. In addition the displacement of the foil $h(x,t)$, measured in the orthogonal (x,z) co-ordinate system, where the x direction is tangential to the path, has to be small $(h(x,t)/c \ll 1)$. These two statements actually limit the chordwise downwash velocity $w(x,t)$ such that $w(x,t)/V(t) \ll 1$, where $V(t)$ is the velocity of the point P, i.e. the local angle of attack of each point along the foil is small. With the above definition the continuity equation in a stationary inertial co-ordinate system (x^*, z^*) (figure 1) is

$$\nabla^2 \phi^* = 0, \tag{1}$$

where ϕ^* is the time-dependent velocity potential due to the foil motion and its wake. This potential can be separated into the plate disturbance potential ϕ_0^* and the wake potential ϕ_w^*, assumed to consist of distributed vortices situated on a deforming sheet (see figure 1):

$$\phi(x^*, z^*, t^*) = \phi_0^* + \phi_w^* \equiv \phi^*. \tag{2}$$

The boundary conditions for (1) are as follows.

(a) There is no flow through the plate surface $z^* = h(x^*, t^*)$:

$$\left.\frac{\partial \phi^*}{\partial z^*}\right|_{\text{on foil}} = \frac{\partial \phi^*}{\partial x^*}\frac{\partial h(x^*,t^*)}{\partial x^*} + \frac{\partial h(x^*,t^*)}{\partial t^*}. \tag{3}$$

(b) The disturbance decays far from the plate:

$$\nabla \phi^* \to 0 \quad \text{as} \quad |x^*|, |y^*|, |z^*| \to \infty. \tag{4}$$

The instantaneous strength of the vortex sheet leaving the foil's trailing edge can be calculated by Kelvin's theorem:

$$\frac{d\Gamma}{dt} = \frac{d\Gamma_f}{dt} + \frac{d\Gamma_w}{dt} = 0 \quad (\text{at all } t), \tag{5}$$

where Γ_f and Γ_w are the foil and wake circulations, respectively.

The instantaneous pressure P at each point on the airfoil is calculated from Bernoulli's equation:

$$\frac{P_\infty - P}{\rho} = -\frac{1}{2}\left[\left(\frac{\partial \phi^*}{\partial x^*}\right)^2 + \left(\frac{\partial \phi^*}{\partial z^*}\right)^2\right] + \frac{\partial \phi^*}{\partial t^*}. \tag{6}$$

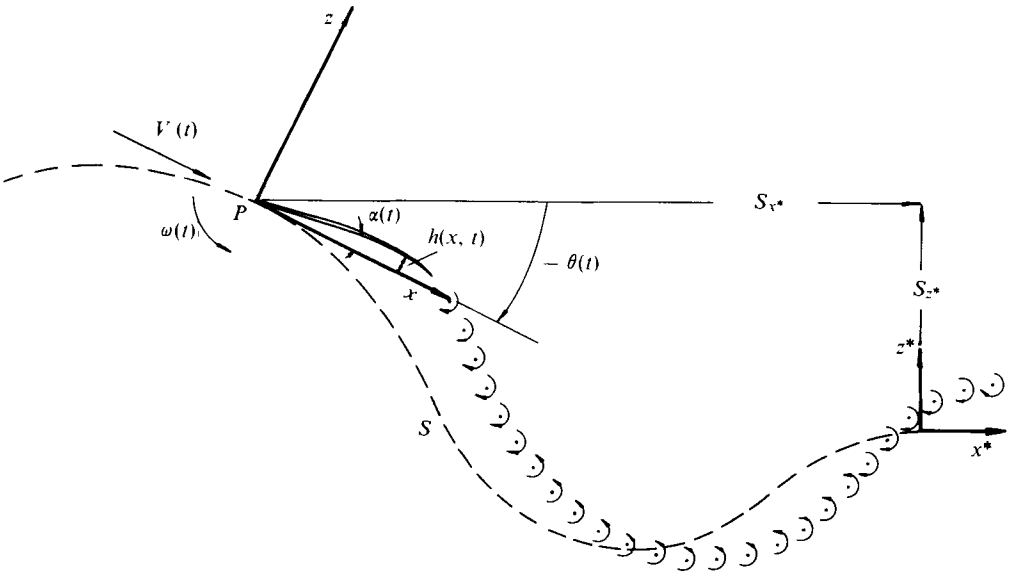

FIGURE 1. Schematic description of model.

The solution of the boundary-value problem (1)–(4) is very complicated owing to the foil surface condition (3). This difficulty is overcome by transforming the problem, which has been stated in the inertial frame of reference (x^*, z^*), into a system (x, z), where the boundary condition on the foil surface is more easily stated. This transformation is

$$\left.\begin{aligned} x &= \cos[\theta(t)]\,[x^* - S_{x^*}(t)] + \sin[\theta(t)]\,[z^* - S_{z^*}(t)], \\ z &= -\sin[\theta(t)]\,[x^* - S_{x^*}(t)] + \cos[\theta(t)]\,[z^* - S_{z^*}(t)], \\ t &= t^*, \end{aligned}\right\} \tag{7}$$

where θ is the inclination of the (x, z) co-ordinate system relative to the (x^*, z^*) frame and (S_{x^*}, S_{z^*}) are the path components (see figure 1). The transformed continuity equation is

$$\nabla^2\phi = 0, \tag{8}$$

$$\phi(x, z, t) = \phi_0 + \phi_w \equiv \phi. \tag{9}$$

The potential ϕ is defined only in the inertial (x^*, z^*) system because definition of a non-rotational velocity potential in the rotating frame (x, z) is impossible. Therefore the derivatives $\partial\phi/\partial x$ and $\partial\phi/\partial z$ are the velocities parallel to the x and z directions as measured in the (x^*, z^*) system.

The transformed boundary conditions are

$$\left.\frac{\partial\phi_0}{\partial z}\right|_{z=0} = \left[V(t) + \frac{\partial\phi_0}{\partial x} + \frac{\partial\phi_w}{\partial x}\right]\frac{\partial h(x,t)}{\partial x} + \frac{\partial h(x,t)}{\partial t} - \frac{\partial\phi_w}{\partial z} + \omega x \equiv W(x, t), \tag{10}$$

where ω is the time-dependent angular velocity of the (x, z) frame,

$$\nabla\phi_0 \to 0 \quad \text{as} \quad |x|, |y|, |z| \to \infty, \tag{11}$$

$$\frac{P_\infty - P}{\rho} = \left\{[z\omega + V(t)]\frac{\partial}{\partial x} - x\omega\frac{\partial}{\partial z} + \frac{\partial}{\partial t}\right\}\phi - \frac{1}{2}\left[\left(\frac{\partial\phi}{\partial x}\right)^2 + \left(\frac{\partial\phi}{\partial z}\right)^2\right]. \tag{12}$$

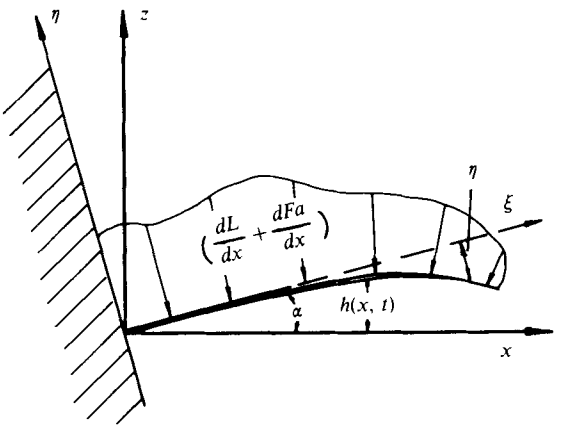

FIGURE 2. Co-ordinate system for calculations of foil bending.

Since the flow disturbances are small compared with the main flow, i.e. $\partial\phi/\partial x$, $\partial\phi/\partial z \ll V(t)$, terms including these derivatives can be neglected.

The above representation of the boundary-value problem has the advantage that the boundary condition on the foil surface [equation (10)] is simpler than (3). This boundary condition is now given in terms of an equivalent instantaneous chordwise downwash $W(x,t)$ that replaces the $V\alpha$ term in steady airfoil theory.

However, in general unsteady motion, the wake potential ϕ_w and the chordwise elastic deformation are not known, so that an iterative solution has to be applied.

3. Calculation of the chordwise elastic deformation

In the present analysis the foil chord is deformed by hydrodynamic pressures and elastic and inertial forces. It is assumed that the foil is clamped at its leading edge and that its elastic behaviour can be estimated by the cantilever model. The calculations are carried out in an orthogonal co-ordinate system (ξ,η) with abscissa along the instantaneous undeflected foil direction, as shown in figure 2.

The deformation of the foil η due to the forces acting on it is obtained from

$$\frac{\partial^2}{\partial\xi^2}\left[E(\xi)\frac{\partial^2\eta}{\partial\xi}\right] = \frac{\partial(P_l-P_u)}{\partial x}\cos\alpha+\frac{\partial F_a}{\partial\xi}, \tag{13}$$

where P_l-P_u is the pressure difference on the airfoil, as obtained from the solution for the potential field, and $E(\xi)$ is the chordwise elasticity factor defined as the product of the local moment of inertia and Young's modulus. The influence of the x component of the force on the foil bending is neglected here. The inertial force distribution $\partial F_a/\partial\xi$ can be calculated by the present method. However, to enable comparison with existing work (Chopra 1976; and others), a massless foil is assumed in the presentation of the results. The instantaneous deflexion $h(x,t)$ of the airfoil produced by the varying angle of attack and the chordwise flexibility is written as

$$h(x,t) = -x\sin[\alpha(t)]+\eta(\xi,t)\cos[\alpha(t)]. \tag{14}$$

The elastic behaviour of the airfoil is found from (13), which is solved as follows. First, a deflexion of the plate $\eta_i(\xi,t)$ (usually the solution at the previous time step) is

assumed and the boundary condition on the plate is calculated from (14) and (10). The potential ϕ_0 is then found as stated before, providing the pressure distribution along the airfoil. This pressure distribution, when substituted in the right-hand side of (13), enables the integration of its left-hand side, resulting in the deflexion of the plate $\eta_{i+1}(\xi, t)$ due to the various forces. If the assumed deflexion η_i and the calculated one η_{i+1} are not identical a correction is made such that

$$\eta_{i+2} = C_1\eta_{i+1} + (1 - C_1)\eta_i, \tag{15}$$

where C_1 is dependent on the chordwise flexibility (usually $C_1 < 0{\cdot}2$). Convergence of the iterative procedure is achieved when $\eta_{i+1} \cong \eta_i$, which usually requires 3–5 iterations. C_1 was selected by trial and error at first.

4. Calculation of the chordwise pressure distribution

The boundary-value problem (8)–(11) is well known (see, for example, Karamcheti 1966, chap. 17) and its solution at any instant is as follows:

$$u(x, 0^{\pm}) = \left.\frac{\partial\phi_0}{\partial x}\right|_{z=\pm 0} = \lim_{z\to 0}\frac{1}{2\pi}\int_0^c \gamma(x_1, t)\,\frac{z}{(x-x_1)^2+z^2}\,dx_1 = \pm\frac{\gamma(x)}{2}, \tag{16}$$

$$w(x, 0^{\pm}) = \left.\frac{\partial\phi_0}{\partial z}\right|_{z=\pm 0} = \lim_{z\to 0}\frac{1}{2\pi}\int_0^c \gamma(x_1, t)\,\frac{x-x_1}{(x-x_1)^2+z^2}\,dx_1 = W(x, t), \tag{17}$$

$$\phi_0(x, \pm 0) = \int_{(0,\,\pm 0)}^{(x,\,\pm 0)} u\,dx = \int_0^x \frac{\gamma(x, t)}{2}\,dx. \tag{18}$$

The solution for the vorticity distribution $\gamma(x, t)$ on the foil is found using the well-known transformation (see, for example, Robinson & Laurmann 1956, chap. 2)

$$x = \tfrac{1}{2}c(1 - \cos\theta_1). \tag{19}$$

It is assumed that the Kutta condition is valid for the unsteady motions dealt with in the present work. Then the vorticity distribution $\gamma(x, t)$ which satisfies (8)–(11) after substitution of (16)–(18) is given in terms of θ_1 by

$$\gamma(\theta_1, t) = 2V(t)\left[A_0(t)\,\frac{1+\cos\theta_1}{\sin\theta_1} + \sum_{n=1}^{\infty} A_n(t)\sin(n\theta_1)\right], \tag{20}$$

where the time-dependent Fourier coefficients $A_0, A_1, \ldots$ are calculated from (17) and found to be

$$A_0(t) = \frac{-1}{\pi}\int_0^{\pi}\frac{W(x, t)}{V(t)}\,d\theta_1, \tag{21}$$

$$A_n(t) = \frac{2}{\pi}\int_0^{\pi}\frac{W(x, t)}{V(t)}\cos(n\theta_1)\,d\theta_1 \quad (n \geqslant 1). \tag{22}$$

The pressure distribution about the airfoil is now found from (12). The terms including the angular velocity ω are symmetric on either side of the foil and do not contribute to the lift distribution dL/dx:

$$\frac{dL}{dx}(x, t) = P_l - P_u = 2\rho\left[\frac{\partial\phi}{\partial t} + V(t)\frac{\partial\phi}{\partial x}\right]. \tag{23}$$

The total lift in the (x, z) system is found by integrating the pressure distribution over the foil, neglecting the wake-influenced parallel velocity relative to the foil near its surface ($\partial\phi_w/\partial x \ll \partial\phi_0/\partial x$, $\partial\phi_w/\partial t \ll \partial\phi_0/\partial t$ on the foil):

$$\begin{aligned} L(t) &= 2\rho \int_0^c \left[\frac{\partial\phi_0}{\partial t} + V(t)\frac{\partial\phi_0}{\partial x}\right] dx \\ &= \pi\rho c \left\{\left[A_0(t)\, V(t)^2 + \frac{3c}{4}\frac{d}{dt}[A_0(t)\, V(t)]\right] + \left[\tfrac{1}{2}A_1(t)\, V(t)^2 + \frac{c}{4}\frac{d}{dt}[A_1(t)\, V(t)]\right] \right. \\ &\quad \left. + \left[\frac{c}{8}\frac{d}{dt}(A_2(t)\, V(t))\right]\right\}. \end{aligned} \tag{24}$$

Similarly, the moment at the leading edge is

$$\begin{aligned} M_y(t) &= -2\rho \int_0^c \left[\frac{\partial\phi_0}{\partial t} + V(t)\frac{\partial\phi_0}{\partial x}\right] x\, dx \\ &= -\frac{\pi}{2}\rho c^2 \left\{A_0(t)\frac{V(t)^2}{2} + \frac{c}{2}\frac{d}{dt}[A_0(t)\, V(t)] + A_1(t)\frac{V(t)^2}{2} + \frac{3c}{16}\frac{d}{dt}[A_1(t)\, V(t)] \right. \\ &\quad \left. - A_2(t)\frac{V(t)^2}{4} + \frac{c}{8}\frac{d}{dt}[A_2(t)\, V(t)] - \frac{c}{16}\frac{d}{dt}[A_3(t)\, V(t)]\right\}. \end{aligned} \tag{25}$$

5. The vortex wake

In order to deal with more general unsteady motions of the foil, and to enable study of wake distortion, a wake model consisting of discrete vortices is constructed (figure 1). At a given time step the wake vortices (or ϕ_w) are known from previous time steps, except for the latest vortex. The strength of this vortex is calculated from (5), where the sum of the distributed vortices replaces the term Γ_w:

$$\frac{d\Gamma}{dt} = \frac{d\Gamma_f}{dt} + \frac{d\left(\sum_{n=0}^{i} \gamma_n\right)}{dt} = 0, \tag{26}$$

where $\gamma_1, \gamma_2, \ldots, \gamma_i$ are the vortices constituting the wake Γ_w. Thus

$$\gamma_i = \frac{\Delta\left(\sum_{n=0}^{i} \gamma_n\right)}{\Delta t} = -\frac{\Delta\Gamma_f}{\Delta t}, \tag{27}$$

where the foil circulation Γ_f is found to be

$$\Gamma_f(t) = \int_0^c \gamma(x)\, dx = V(t)\,[A_0(t)\,\pi + A_1(t)\,\tfrac{1}{2}\pi]. \tag{28}$$†

The instantaneous bound vortex strength Γ_f is dependent on the influence of the wake (including the last vortex) through boundary condition (10). The strength of the most recently shed vortex was therefore calculated iteratively by the Newton–

† The values of ϕ, Γ and their derivatives are defined in the inertial frame of reference (x^*, z^*), as the non-inertial system (x, z) is used mainly to perform the integrations via the transformations suggested.

Raphson method. Convergence within 0·1 % was obtained within three or four iterations.

Another important feature of the above wake model is that after each time step its distortion as a result of the velocity field induced by the foil and its wake may be easily calculated. In cases where the foil did not come close to its own wake the influence was usually found to be negligible (Katz & Weihs 1978).

6. Estimation of performance of harmonic oscillatory propulsor

The mathematical model derived in §§ 2–5 is used to calculate the performance of a flexible, large amplitude oscillating propulsor whose frequency Ω and amplitude H are constant. First the instantaneous forces in the x and z directions are calculated:

$$\Sigma F_x = -\int_0^c \left(\frac{dL}{dx}+\frac{\partial F_a}{\partial x}\right)\frac{\partial h(x,t)}{\partial x}\,dx + T_s, \tag{29}$$

$$\Sigma F_z = \int_0^c \left(\frac{dL}{dx}+\frac{\partial F_a}{\partial x}\right)dx, \tag{30}$$

$$\Sigma M_y = \int_0^c \left(\frac{dL}{dx}+\frac{\partial F_a}{\partial x}\right)x\,dx. \tag{31}$$

Here T_s is the leading-edge suction force and is found from its definition (Robinson & Laurmann 1956, chap. 2)

$$T_s = -\pi\rho K^2, \tag{32}$$

where

$$K = \lim_{x+iz\to 0}(x+iz)^{\frac{1}{2}}u = A_0(t)\,V(t)\,c^{\frac{1}{2}}. \tag{33}$$

Substituting (33) in (32) gives

$$T_s = -\pi\rho c[A_0(t)\,V(t)]^2. \tag{34}$$

Now, if the 'vehicle' is moving in the $-x^*$ direction with speed U_∞ and the propulsor is performing a heaving and pitching motion with frequency Ω, the path parameters can be written as

$$S_{x^*} = -U_\infty t, \tag{35}$$

$$S_{z^*} = (H/c)\sin(\Omega t), \tag{36}$$

$$\alpha = \alpha_1 + \alpha_0 \sin(\Omega t - \varphi), \tag{37}\dagger$$

$$\theta = \tan^{-1}\left[\frac{dS_{x^*}}{dt}\Big/\frac{dS_{z^*}}{dt}\right], \tag{38}$$

$$\omega = d\theta/dt. \tag{39}$$

The propulsive efficiency η_p and the thrust coefficient are defined as

$$\eta_p = \frac{\frac{1}{\tau}\int_0^\tau \left\{(\Sigma F_x\cos\theta - \Sigma F_z\sin\theta)\frac{dS_{x^*}}{dt}\right\}dt}{\frac{1}{\tau}\int_0^\tau \left\{(\Sigma F_x\sin\theta + \Sigma F_z\cos\theta)\frac{dS_{z^*}}{dt} + M_y\frac{d(\alpha+\theta)}{dt}\right\}dt}, \tag{40}$$

$$C_T = \frac{2}{\rho U_\infty^2 c}\frac{1}{\tau}\int_0^\tau (\Sigma F_x\cos\theta - \Sigma F_z\sin\theta)\,dt, \tag{41}$$

where τ is a whole number of periods of oscillation.

† Notice that α is measured anticlockwise (figures 1 and 2).

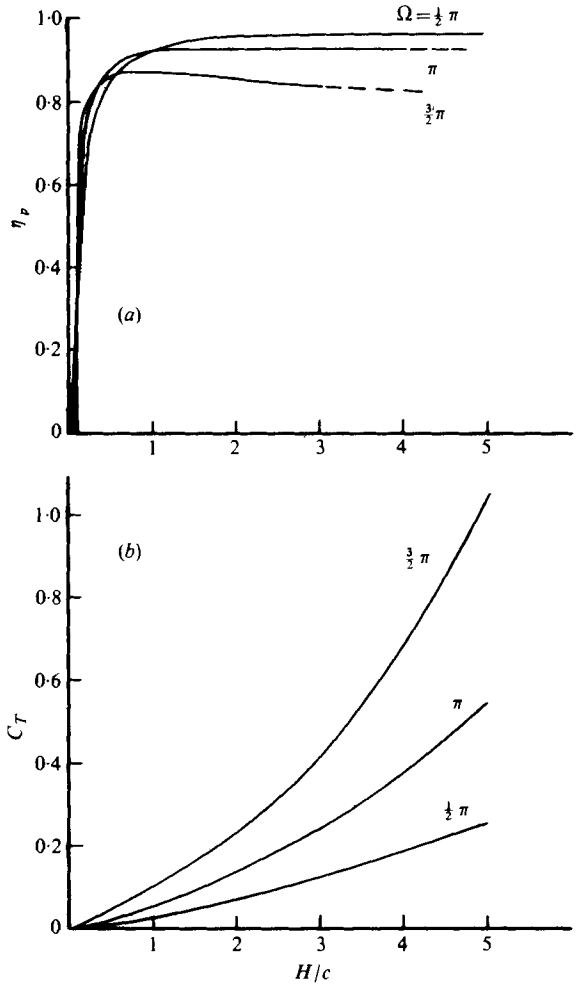

FIGURE 3. The influence of the amplitude ratio and frequency on (*a*) the efficiency and (*b*) the thrust coefficient. $U_\infty/c = 10\ \mathrm{s}^{-1}$, $\alpha_0 = 5°$, $\varphi = \frac{1}{2}\pi$.

7. Discussion of results

Large amplitude rigid propulsor

The most important feature of oscillatory propulsion is that the thrust grows as the amplitude ratio H/c increases (figure 3). This was pointed out by Chopra (1976), whose results are similar to the present ones, although in his model the vortex wake was not allowed to deform in the induced velocity field. This leads to the conclusion that the vortex wake deformation may be neglected in modestly oscillating motions,

$$\sigma = \tfrac{1}{2}\Omega c/U_\infty < 0{\cdot}3.$$

The dashed lines in figure 3 (*a*) represent a region where the local chordwise downwash is higher ($\omega c/V(t)\,\alpha_{\max} \geqslant 1$)† than is permitted by the linear theory (separation

† α_{max} was taken to be the maximal angle of attack, just before separation occurs.

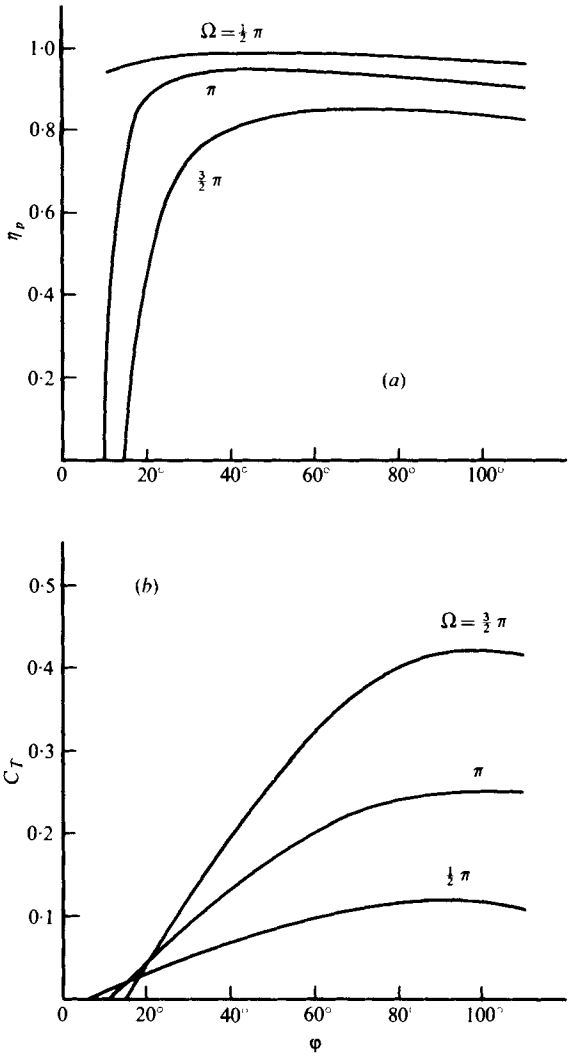

FIGURE 4. The influence of the phase difference φ on (*a*) the efficiency and (*b*) the thrust coefficient. $U_\infty/c = 10\ \mathrm{s}^{-1}$, $H/c = 3$, $\alpha_0 = 5°$, $\varphi = \frac{1}{2}\pi$.

is expected). This usually occurs after peaks in the sinusoidal motion and can strongly affect the calculation of the efficiency, as predicted by Chopra (1976).

Figure 3 shows the increase in thrust when the frequency is raised. The same behaviour is obtained when the maximum angle of attack α_0 is increased (e.g. Chopra 1976). The theoretical efficiency is very high, as indicated in figures 3–5. As the path curvature rises (i.e. Ω grows), the effort exerted in the foil pitching at the extremes of the sinusoidal motion grows. For that reason the efficiency slightly decreases, as indicated in figure 3. One possible way to overcome this loss is to change the pitching axis, as pointed out by Lighthill (1970) and Chopra (1974); see also figure 5(*a*).

Most of the studies (Scherer 1968; Chopra 1974, 1976) dealing with oscillatory propulsion assume a phase difference of $\frac{1}{2}\pi$ between the heaving and pitching motions.

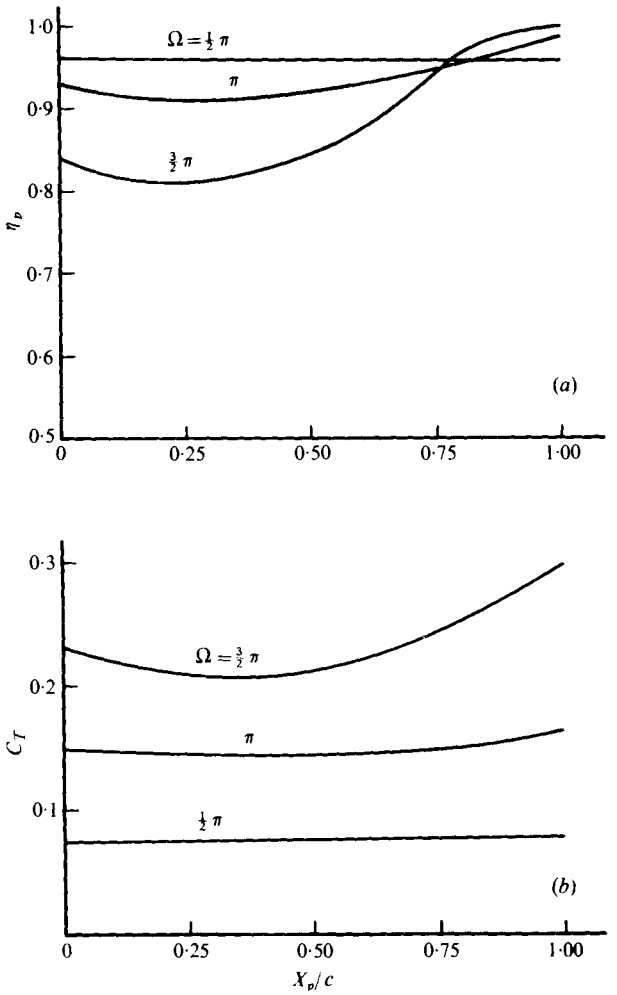

FIGURE 5. The influence of the location of the pitching axis on (*a*) the efficiency and (*b*) the thrust coefficient. $U_\infty/c = 10\ \mathrm{s}^{-1}$, $H/c = 2$, $\alpha_0 = 5°$, $\varphi = \frac{1}{2}\pi$.

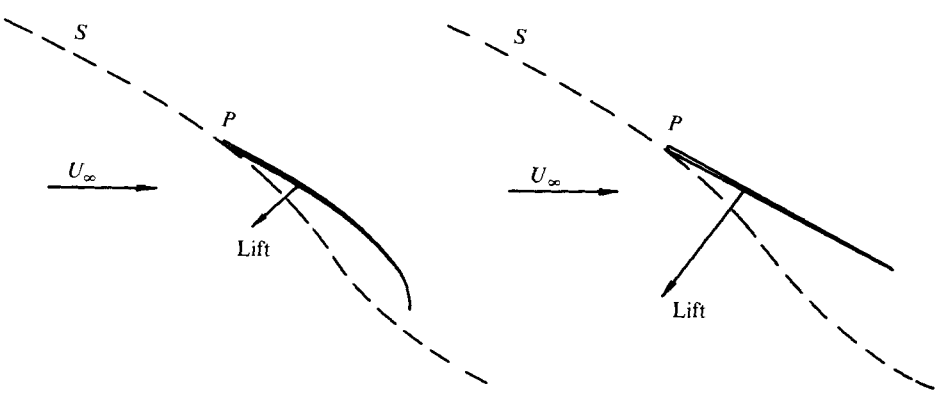

FIGURE 6. The influence of flexibility on the instantaneous lift of a propulsor foil.

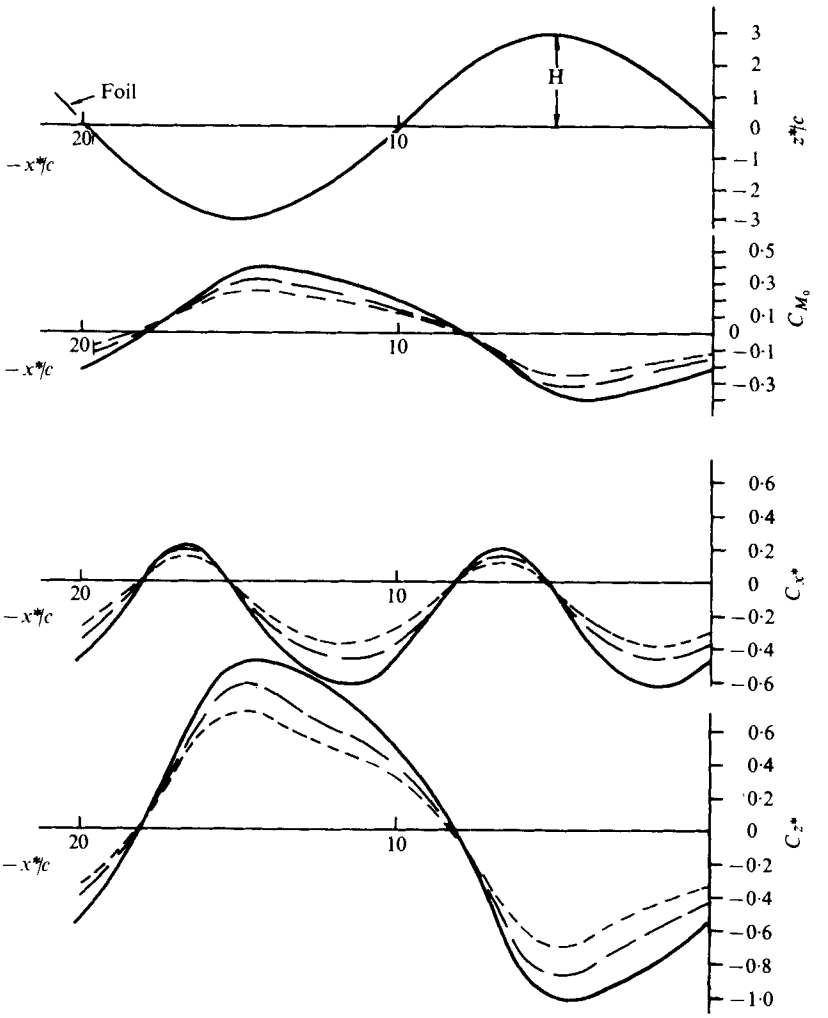

FIGURE 7. Variation of moments and forces during periodic motion of a flexible foil. ——, $E/T_r c^2 = \infty$; — — —, $E/T_r c^2 = 100$; - - -, $E/T_r c^2 = 50$. $U_\infty/c = 10\ \mathrm{s}^{-1}$, $H/c = 3$, $\alpha_0 = 5°$, $\Omega = \pi$, $\varphi = \frac{1}{2}\pi$.

Figure 4 shows that around $\varphi = 90°$ both the thrust and the efficiency are very high, as found experimentally by Scherer (1968).

The effect of the location x_p of the pitching axis on the efficiency and the thrust coefficient is indicated in figure 5. The gain in efficiency as x_p moves in the $+x$ direction is mainly due to the decrease in the work required to turn the foil when the heave amplitude is near its maximum. This figure shows quantitatively the point made by Lighthill (1970), that the pitching axis should be located in the rear quarter of the foil. Investigation of the influence of varying the average angle of attack α_1 (over the range $-15° < \alpha_1 < 15°$) showed, in the present case of a two-dimensional foil, that α_1 has no significant effect on the thrust and efficiency.

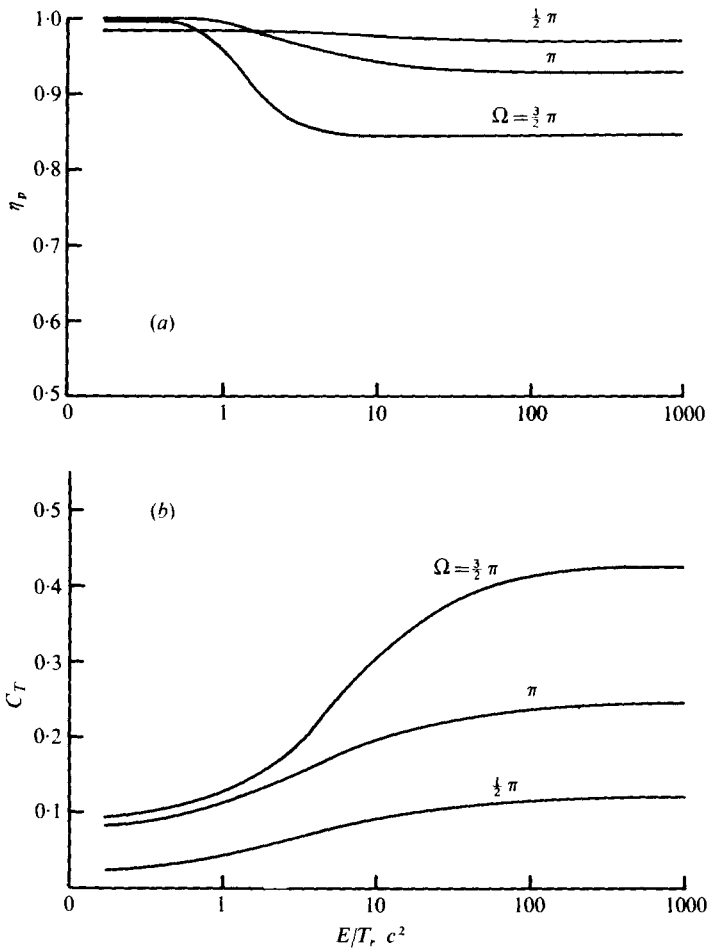

FIGURE 8. The influence of flexibility on (*a*) the efficiency and (*b*) the thrust coefficient. $U_\infty/c = 10\ \mathrm{s}^{-1}$, $H/c = 3$, $\alpha = 5°$, $\varphi = \frac{1}{2}\pi$.

The influence of chordwise flexibility on large amplitude oscillatory propulsion

The main effect of chordwise flexibility on oscillatory propulsion is demonstrated in figure 6. The fin chord is distorted owing to the hydrodynamic pressures, and the overall instantaneous lift decreases. On the other hand, the orientation of the resultant lift is nearer the direction of advance, therefore a higher efficiency can be expected. In the results presented here a uniform chordwise flexibility distribution ($E(\xi)$ = constant) and a massless† thin foil are assumed. However, the method derived in the present study can include chordwise variations in flexibility and a mass distribution.

The periodic variation of the forces during the foil motion is represented in figure 7, which shows the variation of the forces and moments on the foil during a typical cycle for various values of the flexibility parameter $E/T_r c^2$. This parameter describes the

† The frequency of the motion here is very low relative to the mechanical resonance of the propulsor, so that its performance can be predicted by assuming a massless plate.

relative distortion of the profile shape during a specific motion, T_r being the average thrust of a rigid propulsor of chord c performing the same periodic motion. The full line represents the case of a rigid foil while the dashed lines give the results for flexible foils. In general, chordwise flexibility does not change the variation of the forces within a period, but reduces their magnitudes. The above behaviour of the forces and moments is very similar to Scherer's (1968) experimental results, which were obtained with a propulsion fin of aspect ratio 3.

The influence of chordwise flexibility on the propulsive efficiency and thrust is seen in figure 8. As stated before, slight flexibility can lead to a moderate gain in efficiency with a loss in thrust that is still tolerable. This phenomenon was observed qualitatively by Picken & Crowe (1974), who compared the performance efficiency of various swim-fins. For very flexible propulsors the efficiency is even higher, but the thrust is reduced below practical levels.

REFERENCES

Bonthron, R. J. & Fejer, A. A. 1962 A hydrodynamic study of fish locomotion. *Proc. 4th U.S. Nat. Cong. Appl. Mech., Berkeley, California*, pp. 1249–1255.

Chopra, M. G. 1974 Hydromechanics of lunate-tail swimming propulsion. *J. Fluid Mech.* **64**, 375–391.

Chopra, M. G. 1976 Large amplitude lunate-tail theory of fish locomotion. *J. Fluid Mech.* **74**, 161–182.

Giesing, J. P. 1968 Nonlinear two dimensional unsteady potential flow with lift. *J. Aircraft* **5** (2), 135–143.

James, E. C. 1973 A linearized theory for the unsteady motions of a wing in curved flight. *Naval Ship. R. & D. Center, Bethesda, Maryland, Rep.* no. 4098.

Karamcheti, K. 1966 *Principles of Ideal-Fluid Aerodynamics.* Wiley.

Katz, J. & Weihs, D. 1978 The effect of chordwise flexibility on the lift of a suddenly accelerated airfoil. (To appear.)

Lighthill, M. J. 1960 Note on the swimming of slender fish. *J. Fluid Mech.* **9**, 305–317.

Lighthill, M. J. 1970 Aquatic animal propulsion of high hydromechanical efficiency. *J. Fluid Mech.* **44**, 265–301.

Lighthill, M. J. 1971 Large amplitude elongated body theory of fish locomotion. *Proc. Roy. Soc.* B **179**, 125–138.

Picken, J. & Crowe, C. T. 1974 Performance efficiency of swim-fins. *Ocean Engng* **2**, 251–258.

Robinson, A. & Laurmann, J. A. 1956 *Wing Theory.* Cambridge University Press.

Scherer, J. O. 1968 Experimental and theoretical investigation of large amplitude oscillating foil propulsion systems. *Hydronautics Inc. Tech. Rep.* no. 662–1.

Siekmann, J. 1962 Theoretical studies of sea animal locomotion. Part 1. *Ing. Arch.* **31**, 214–228.

Siekmann, J. 1963 Theoretical studies of sea animal locomotion. Part 2. *Ing. Arch.* **32**, 40–50.

Webb, P. W. 1975 Hydrodynamics and energetics of fish propulsion. *Fisheries Res. Bd Can. Bull.* no. 190.

Wu, T. Y. 1961 Swimming of a waving plate. *J. Fluid Mech.* **10**, 321–344.